Magnetic behavior of magneto-rheological foam under uniaxial compression strain

Gildas Diguet, Gaël Sebald, Masami Nakano, Mickaël Null Lallart, Cavaillé J.-Y.

Magnetic behavior of Magneto-Rheological Foam under Uniaxial Compression Strain

Gildas Diguet[1,2,3], Gaël Sebald[1], Masami Nakano[1,4], Mickaël Lallart[1,2,5], Jean-Yves Cavaillé[1]

[1] ELyTMaX UMI 3757, CNRS-Université de Lyon-Tohoku University International Joint Unit, Tohoku University, Sendai, Japan
[2] Institute of Fluid Science, Tohoku University, Sendai, Japan
[3] Division for the Establishment of Frontier Sciences, Organization for Advanced Studies, Tohoku University, Sendai, Japan
[4] New Industry Creation Hatchery Center, Tohoku University, Sendai, Japan
[5] Univ. Lyon, INSA-Lyon, LGEF EA682, F69621 Villeurbanne, France

E-mail: gildas.diguet.d4@tohoku.ac.jp

Received xxxxxx
Accepted for publication xxxxxx
Published xxxxxx

Abstract

This study reports the development of a Magneto-Rheological Foam, which consists in a porous matrix filled by ferromagnetic particles. The porous matrix of such a composite being easily deformable, large magnetic properties changes are expected. The measurements of the magnetic properties of such a Magneto-Rheological Foam submitted to a compressive strain are reported. Main aspect of the magnetic properties is the low field magnetic permeability as the function of the compression and filling factor. Then, larger field magnetization measurement allowed to investigate the saturation field as a function of the filling factor. Because of the large amount of pores in the material, the magnetic relative permeability, μ_r, is quite small ($\mu_r \sim 1$). However, these materials can be easily deformed over a large range of strain providing important relative variation of the magnetic properties under mechanical solicitation. The composite magnetic permeability is increasing under compression for all the considered filling factors. A model is then developed to understand the variation of the permeability with the strain. Hence, from a simple concept consisting of taking advantage of high deformation of foams, the present study demonstrates the interest of such a highly compressible while cheap composite for obtaining a large magneto-rheological effect.

Keywords: Magnetic Composite, permeability, uniaxial compression, Poisson ‘ratio, foam

1. Introduction

Most of the commonly studied magnetic composites consist of well-known Magneto-Rheological Elastomers [1-2] (MREs) and Magneto-Rheological Fluids [3] (MRFs). Such MREs (resp. MRFs), having a relatively low Young modulus in the order of a few MPa (resp. Low viscosity), are highly studied for their ability to control the mechanical properties (elasticity or viscosity for instance) through the application of a magnetic field. Such magnetic fields are magnetizing the (magnetically) soft ferromagnetic particles, which are then interacting with each other. In the case of MRF, some chains are formed along the magnetic field direction [4] and these interacting particles are counteracting any shear strain mechanically applied perpendicularly to the chain, yielding a

MR effect. Typical application of such a phenomenon consists of magnetically tunable damping systems. Similar effect is also observed in the viscoelastic behavior of the MRE. Another aspect is the deformation along the magnetic field axis [5-7] of the MRE, namely magnetostriction, yielding strains up to 10%, as the magnetic field is applied. In the case of the MRF, the surface tension is in competition with the magnetic interaction [8] to produce wrinkles on the liquid surface. Apparent change of mechanical properties and deformation under magnetic field are two phenomena resulting from the magneto-elastic coupling effect. Furthermore, these materials can also exhibit reverse effects: the observation of the change in magnetic properties due to a mechanical solicitation, leading to the rise of a voltage across a pick-up coil for instance ([9-11]).

As the most direct application of MR effect targets magnetic damper systems, most of the works investigating MREs are focusing on the magnetic to mechanical conversion whereas the inverse effect is poorly studied. Recently, energy harvesting application using MREs submitted to a shear strain has been proposed to this end [9-11]. In these works, the MRE has been prepared by curing the matrix under an applied magnetic field which produced the alignments of particles thus inducing effective anisotropy of magnetic [12-13] and elastic [14] properties. As such MREs were strained by application of a shear excitation γ, the magnetic permeability μ experienced a change in its value [15-16]. Such a permeability modification $\Delta\mu(\gamma)=\mu(\gamma)-\mu(\gamma=0)$, together with an applied field, thus produces a change of induction which is later converted into an electric signal through a coil for energy harvesting application. To achieve larger effect, larger strain is required. The principle of changing the silicone rubber matrix of the MRE using a PolyUrethane foam which, in spite of its simplicity, was poorly considered so far, thus enables easy achievement of such large deformations. Beside, the change of shear induction, $\Delta B(\gamma)=B(\gamma)-B(\gamma=0)$, was weakly dependent on the choice of the matrix in the case of MRE [9]. A large compression dependent magnetic permeability can thus be expected for MR foams. This therefore opens new application routes thanks to the high deformability of such materials potentially allowing high coupling between magnetic and mechanical properties.

While some works already investigated Magneto-Rheological Foams, with the aim to produce a composite with a low elastic modulus, and to observe the MR effect (change of elastic properties with the application of the magnetic field) [17-18], they mainly focused on the magnetic to mechanical coupling. Ju el al. [19] have manufactured a so-called Porous MRE, P-MRE, where porosity was controlled by the quantity of added ammonium bicarbonate (NH4HCO3) which were decomposing in CO2 as the MRE was cured. A P-MRE without porosity exhibited a storage modulus of $G(B=0)$=2 MPa whereas P-MRE with a porosity of 35% showed a storage modulus of $G(B=0)$=0.74 MPa. With the application of a magnetic flux density of B=600 mT, the MR effect (($G(B>0)$-$G(B=0)$)/$G(B=0)$) showed remarkable values up to 170% for the porous material compared to 25 % for the non-porous case. It was pointed out that the loss factor increased with the porosity, however. Another work performed by Gong et al. in the framework of magnetically adaptable acoustic absorption has shown an even stronger MR effect when considering anisotropic MR foams [20]. A recent work [21] has shown a lower shear modulus G' for a composite based on Ethylene propylene diene rubber (EPDM) and Carbonyl Iron Particles when foaming agent (activated azodicarbonate) was used but this reduction of modulus was accompanied by a lower MR effect; the authors suggested that pore increased the inter-particles distance and the interaction, reponsible for the MR effect, was lower. Magnetic foams can also be used to tune electric properties by compression [22]: a 7 wt.% filled anisotropic MRE electric conductivity was increased from 10^{-8} S/cm to 10^{-7} S/cm by reducing the inter-particle distance of in the composite.

In this article, we propose to focus on the converse effect, namely the dependence of the magnetic characteristics on the mechanical state of the material. The manufactured materials are based on a highly porous matrix, with different quantity of magnetic particles. Change of magnetic permeability $\Delta\mu(\varepsilon)=\mu(\varepsilon)-\mu(\varepsilon=0)$ with applied mechanical compression ε is then revealed and discussed with respect to the filling factor and the strain strength.

2. Experimental

1.1 Sample production

The Magneto-Rheological Foam samples were obtained from commercial products both for the foam and the Fe particles, regarding their processability. The PolyUrethane (PU) matrix was obtained from a commercial foam, FlexFoam-IT III from Smooth-on, Inc. It is a bi-component (part A : the isocyanate and part B : the polyol phase [23]) PU foam which has to be mixed according to the preconized weight ratio A:B = 57:100 and stirred for 30 seconds. Fe particles have been purchased from BASF: Carbonyl Iron Particles C3518 which have an average diameter of 5 µm. Each component (A, B, Fe) and sample masses were measured using a chemical scale Sefi ITX220 from AsOne with a sensitivity of 100 µg. First, Fe particles were injected to the A component and mixed, then the B component was added to the mixture and the whole mixture was then stirred for 30 seconds. Final mixture was then left at room temperature to complete the foam expansion overnight.

Table1. Mass of the components (A, B and Fe) for manufacturing the magnetic foam, and the samples final dimensions and masses for permeability measurements and VSM measurements respectively.

Preparation						Samples for Permeability meas.		Samples for VSM meas.	
ID	m_A (g)	m_B (g)	m_{Fe} (g)	m_A/m_B	$m_{Fe}/(m_A+m_B+m_{Fe})$ (wt.%)	dimension (mm)	mass (g)	dimension (mm)	mass (g)
#1	2.0221	3.5759	0.0000	0.57	0.00	38.1*34.5*19.8	2.1971	6.5*6.2*2.9	0.0088
#2	2.0211	3.4934	1.0593	0.58	16.11	36.9*35.8*13.9	2.1475	6.0*5.0*3.4	0.0123
#3	1.9553	3.4438	2.0170	0.57	27.20	37.5*33.4*16.3	2.3746	6.0*5.5*3.4	0.0150
#4	1.9886	3.4659	3.1993	0.57	36.97	39.3*34.6*14.6	3.0178	6.6*6.3*3.9	0.0214
#5	1.9843	3.4619	4.3649	0.57	44.49	37.0*35.5*18.7	3.7886	6.8*6.0*3.3	0.0218
#6	2.0020	3.5010	6.3496	0.57	53.57	35.5*34.4*18.4	4.0165	6.3*6.0*4.0	0.0283
#7	2.0237	3.4610	9.0089	0.58	62.16	35.3*35.6*15.5	4.4265	6.8*5.1*4.0	0.0340
#8	2.0246	3.5146	12.0857	0.58	68.57	38.2*29.2*15.7	6.3556	5.3*5.0*3.3	0.0302

Using the above-described procedure, several composites were manufactured with different Fe mass content. Samples were cut into rectangular blocks for direct permeability measurements; size and masses of the corresponding samples are gathered in Table 1. For Vibrating Sample Magnetometer (VSM) measurements, smaller sample size is required. In fact, after cutting the samples for the purpose of permeability measurements, the removed parts were then reused for VSM. These cut part were reshaped as small rectangular blocks; information on the masses and dimensions are given in Table 1.

Table2. Extracted values of susceptibilities, magnetic saturation from VSM measurements, along with filling factor of the MR Foams obtained by densities and magnetic saturations.

ID	χ (-)	χ_{corr} (-)	M_{sat} (kA/m)	ϕ_{Fe} (vol.%) from ρ	ϕ_{Fe} (vol.%) from M_{sat}
#1	-9.6×10^{-5}	-9.6×10^{-5}	-	0.00	0.00
#2	1.24×10^{-2}	1.25×10^{-2}	5270	0.24	0.27
#3	2.55×10^{-2}	2.59×10^{-2}	10349	0.40	0.50
#4	4.16×10^{-2}	4.26×10^{-2}	16233	0.71	0.83
#5	5.31×10^{-2}	5.48×10^{-2}	20382	0.87	1.02
#6	9.07×10^{-2}	9.57×10^{-2}	34729	1.22	1.61
#7	14.13×10^{-2}	15.35×10^{-2}	53020	1.80	2.43
#8	19.22×10^{-2}	21.42×10^{-2}	68014	3.17	3.54

In Fig.1, an example of the surface of samples, observed with an Olympus SZX9 Stereo Microscope, is presented to show that the obtained typical foam pores size about 100-1000 µm, which is much larger compared to the micro particles.

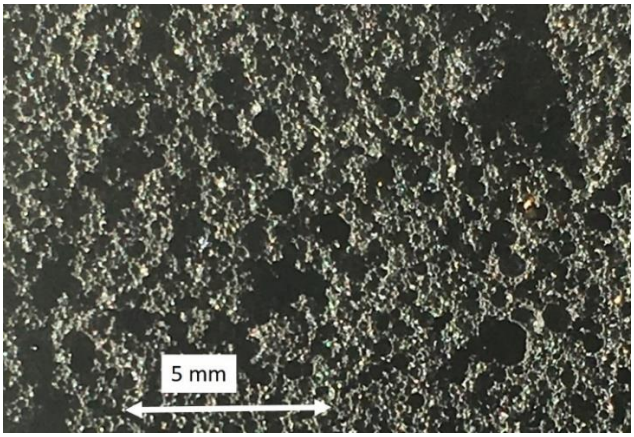

Fig.1. Magneto-Rheological Foam sample #8 surface

1.2 Permeability measurement

For the magnetic characterization, two techniques were used. The first one consisted in investigating the composite relative permeability. The permeabilities of Magneto-Rheological Foam samples were measured using a Magnetic Permeability Meter Ferromaster from Stefan Mayer Instruments. This instrument is capable of measuring the relative permeability in the range of μ_r=1 to 2 with an accuracy of 0.001 [11], which falls well within the expected range of Magneto-Rheological Foams with very low filling factors. The measurements consisted in placing the probe perpendicularly to the tested sample surface while applying a static mechanical solicitation over the whole top surface of the sample (Fig.2a).

The probe of the permeability-meter was placed on top of the tested sample, directed along the compression axis. As the sample thickness is manually reduced and controlled by a Z-stage platform (Fig.2b) the displacements were recorded at each step and the effective compression strain is calculated as $\varepsilon=(h-h_0)/h_0$, with h_0 being the non-deformed sample thickness. The compression was considered as a quasi-static compression.

a

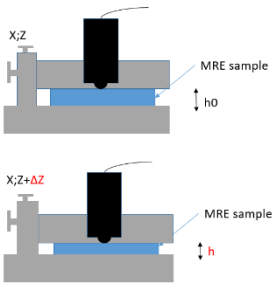

b

*Fig.2.a Set up for measuring the strain-induced permeability. Application of strain is done by lowering the table (area of 44mm*47mm), b) principle of permeability measurement of strain foams*

1.3 Magnetization measurement

Previous investigations focused on the low-field permeability. Hence, high-field characterization is proposed in this section to obtain the quantity of particles in the composite by measuring the saturation of the magnetization curve. To this end, a Vibrating Sample Measurement magnetometer (VSM) was used. The experiments were carried out with a BHV-50H VSM from Riken Denshi Co which is able to apply a magnetic field up to H_0=10 kOe ($\mu_0 H_0$=1 T or H_0=800 kA/m). The device was tested five times using a calibrated rectangular piece of Nickel, showing a measurement error of less than 2%.

As mentioned in the material preparation section, the samples used for VSM measurements were produced from the same batch as the samples used for permeability measurements. However, samples with smaller size were required for the VSM as shown in Table 1. Nonetheless, the samples ID in Table 1 corresponds to the preparation composition and the samples densities (for the two measurements) are close to each other (Fig. 3).

The samples were placed on a holder with a clamping mechanism featuring four screws for tightening. Clamping is necessary because, for this technique, an oscillating displacement is applied to pick a change of flux proportional to the magnetization of the sample. In fact, as the foams are easily deformable,the clamping system was later adjusted to apply the same initial height h_0=3.0 mm for all samples.

1.4 Inductance measurement

In this case, the Permeability Meter was removed and a small coil (L_0=26.47µH, diameter 22 mm) was inserted between test sample and the moving plate in the same device as in Fig.2a. The coil was then connected to a HP4194A Impedance Analyzer, which was acquiring data in R_s-L_s mode. Testing frequency was set at 200 kHz.

2. Results

2.1 Samples density

Densities values, calculated from Tables 1, are plotted in Fig.3 as a function of the relative Fe weight concentration ($m_{Fe}/(m_A+m_B+m_{Fe})$) for the two sets of samples. Both sample sets (for permeability determination and VSM measurements) present similar densities, except for the samples with the highest content of Fe. A threshold is indeed observed as the relative weight concentration of Fe is getting close to 70%. Such discrepancies are explained by the high mass fraction that accentuates dimensional uncertainties and dispersion inhomogeities. The relationship between the density and the relative Fe weight concentration can be modeled as described below.

The composite density ρ can then be obtained by expressing the density as the ratio of the total mass, $m_{tot}= m_A+m_B+m_{Fe}$, to the whole volume (particles and apparent PU foam), as:

$$\rho = \frac{m_{Fe} + m_{PU}}{V_{Fe} + V_{PU\_r}} = \frac{m_{tot}}{\frac{m_{Fe}}{\rho_{Fe}} + \frac{(m_{tot} - m_{Fe})}{\rho_{PU\_r}}} \qquad (1)$$

The density ρ_{Fe} is referring to the Fe density and ρ_{PU_r} to the apparent PU foam density that includes the porosity (PU_r ≡ PU + air).

By inverting Eq.1, we obtained the density as function of the Fe mass to total mass ratio as:

$$\frac{1}{\rho} = \frac{m_{Fe}}{m_{tot}}\left(\frac{1}{\rho_{Fe}} - \frac{1}{\rho_{PU\_r}}\right) + \frac{1}{\rho_{PU\_r}} \qquad (2)$$

The experimental density values in Fig.3 are fitted using Eq.2 with the assumption of ρ_{Fe}= 7874 kg/m3 with the apparent PU foam ρ_{PU_r} being the unknown. The fit process provided a value ρ_{PU_r} ~ 90 kg/m3 which is seen on the Fig.3 for sample #1 which possessed no Fe particles. By comparing this apparent density ρ_{PU_r} to the pure PU density ρ_{PU} ~ 1200 kg/m^3, the foam relative foam density defined as ρ_{PU_r}/ρ_{PU} is estimated to be ~ 10%, which is assumed to be the same for all composites. Such an assumption may however lead to some inaccuracy, especially for sample #8 for instance, as a larger density ρ_{PU_r} than 97 kg/m^3 could explain the larger density of the composite. Such a larger ρ_{PU_r} implies a lower porosity of the foam which might be a consequence of higher Fe contents. Consequently, the sample #8 is assumed to have a lower porosity compared to other samples. It is possible that the higher Fe content has modified the expansion rate of the foam yielding to a lower porosity.

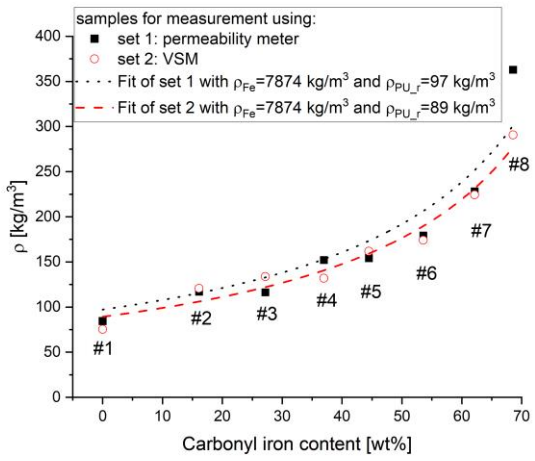

Fig.3. Samples density as function of Fe concentration. Dotted and dashed lines are fitted curves for the two experimental data using Eq.2

2.2 Samples filling factor

The relative Fe weight concentration is a parameter that is experimentally easy to obtain from mass measurements. However, for discussion on the magnetic and/or mechanical properties, the volume fraction of Fe of the composites, also called filling factor, is more important and therefore has to be estimated.

These Magneto-Rheological Foams have three components: polyurethane, air and magnetic particles. Each sample is then characterized by the volume fraction of the three components phase (PU, Fe particles and air) relatively to the whole volume V_{tot} as $\phi_{PU}= V_{PU}/V_{tot}$, $\phi_{air}= V_{air}/V_{tot}$ and $\phi_{Fe}= V_{Fe}/V_{tot}$. In the following, the filling factor is obtained from experimental results with two methods.

2.2.1 From the densities. Starting from the assumption that the masses of PU and Fe remained unchanged during the foam expansion, the mass ratio of Fe to PU remains constant in the process. It is then possible to estimate the volume fraction of Fe (ϕ_{Fe}) in the foam from the mass of samples listed in Table 1 as follow. First, the ratio of Fe to PU is derived as:

$$\frac{m_{Fe}}{m_{PU}} = \frac{V_{Fe}\rho_{Fe}}{V_{PU}\rho_{PU}} = \frac{(V_{Fe}/V_{tot})\rho_{Fe}}{(V_{PU}/V_{tot})\rho_{PU}} = \frac{\rho_{Fe}\phi_{Fe}}{\rho_{PU}\phi_{PU}} \qquad (3)$$

By rewriting the Eq.3, the volume fraction of PU (ϕ_{PU}) is then:

$$\phi_{PU} = \frac{\rho_{Fe}\phi_{Fe}}{\rho_{PU}}\frac{m_{PU}}{m_{Fe}} \qquad (4)$$

As the composite density is the sum all the component densities times their volume fraction, and by neglecting the term ρ_{air}, this density is expressed using the Eq.4 as a function of the volume fraction of Fe:

$$\rho = \rho_{Fe}\phi_{Fe}\left[1 + \frac{m_{PU}}{m_{Fe}}\right] \qquad (5)$$

This Eq.5 is helpful as the volume fraction of Fe, also called filling factor, in each sample is finally isolated and expressed as:

$$\phi_{Fe} = \frac{\rho}{\rho_{Fe}}\left[\frac{m_{Fe}}{m_{Fe} + m_{PU}}\right] \qquad (6)$$

Using data from Table 1, the sample densities are calculated and injected in Eq.6 to estimate the corresponding filling factors, which are reported in the Table 2. This parameter is actually useful for comparing the material properties.

2.2.2 From the Magnetization curves. A second method, based on the composite magnetization curve measurement, is used here to confirm the filling factor of composite obtained by Eq.6. Each samples magnetization curve is presented in the Fig.4 as function of external field *H* and it is clearly observed that the magnetic saturation of composites M_{sat} increases with the content of magnetic particles in the Magneto-Rheological Foam.

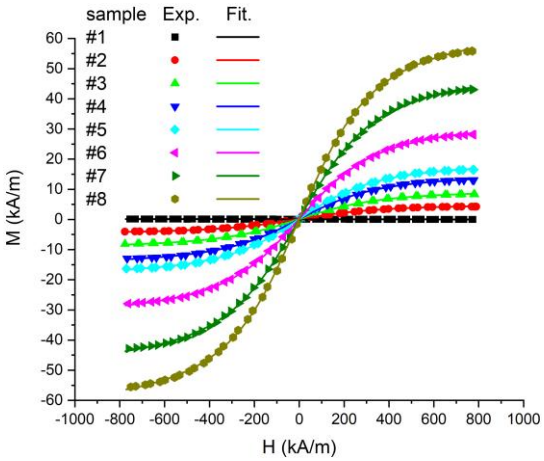

Fig.4. Magnetization versus applied field curve for each Magneto-Rheological Foam without compression

This saturation state (M_{sat}) of the magnetization curve, is obtained when all magnetic moments carried by the Fe

particles are aligned along the applied magnetic field direction. For a composite, this volume quantity [5, 12-13] is relating the value of the filling factor ϕ_{Fe} to the magnetic saturation of the Fe particles M_{sat_Fe} =1735 kA/m [16] as:

$$M_{sat} = \phi_{Fe} M_{sat\_Fe} \quad (7)$$

Values of the magnetic saturation of each composite are extracted from Fig.4 from the Langevin equation [24]:

$$\mathrm{M(H)} = M_{sat}\left[\frac{1}{\tanh\left(\frac{m\mu_0 H}{k_B T}\right)} - \frac{1}{\frac{m\mu_0 H}{k_B T}}\right] \quad (8)$$

where μ_0 is the magnetic permeability of free space (4π x 10^{-7} Hm^{-1}), m is the magnetic moment, H is the applied field, k_B is the Boltzmann constant space (1.38 x 10^{-23} JK^{-1}) and T is the temperature in Kelvin. Saturation (M_{sat}) are reported in Table 2. From these values, the filling factor ϕ_{Fe} is calculated using Eq.7 and the corresponding values are also provided in Table 2. These extracted the filling factor ϕ_{Fe} from the experimental magnetization and from the densities are in same range (Table 2), validating the two approaches.

2.3 Samples permeability

2.3.1 Without compression. The relative permeabilities, without deformation, were measured for each samples. Results are presented in Fig.5 as function of filling factor for each sample, obtained by the average of the values from Table 2 from densities (Eq.6) and magnetic saturation (Eq.7), and the error bars are obtained from these values differences.

Measured relative permeabilities exhibits a linear behavior with the filling factor. The estimated filling factor are relatively small for all the samples tested. This allows the comparison between the experimental results and Maxwell-Garnett (MG) effective susceptibility χ or relative permeability μ_r. This law is indeed used for a random and dilute distribution of ferromagnetic spheres in non-magnetic medium [25] and these hypotheses are satisfied here. This law assumed that particle permeability μ_p is much larger than the surrounding medium μ_m ($\mu_p >> \mu_m$) and the expression of the Maxwell-Garnett permeability expressing μ_r is a simple function of the filling factor and is given as:

$$\mu_r = 1 + \chi = 1 + \frac{3\phi_{Fe}}{1 - \phi_{Fe}} \quad (9)$$

Theoretical results using the Maxwell-Garnett law are also plotted in Fig.5 and show in good agreement with the effective measured permeabilities. Beside it explained the almost linear behavior of permeabilities for these relatively low filling factors.

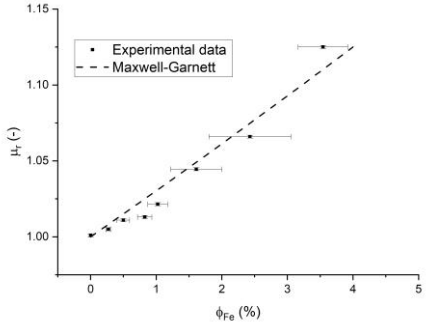

Fig.5. Relative permeabilities of non-deformed Magneto-Rheological Foams as function of volume fraction of Fe particles.

Magneto-Rheological Foams are three components materials with a single randomly distributed magnetic phase, whereas both the matrix and the pore are non-magnetic. However, the samples permeabilities behavior is similar as predicted by the effective medium calculated by Maxwell-Garnett rule for two components. This confirmed that the Magneto-Rheological Foams can be modelled as composites with random distribution of magnetic particles in a non-magnetic material (matrix and air).

From the magnetization versus applied field curves (Fig.4), the magnetic susceptibilities χ are extracted from the slope of the curves close to H=0, as χ=(dM(H=0)/dH). Correction to account the demagnetizing factor is also performed using formula for rectangular cuboid shape samples [26]. As the foam is not strongly magnetic, this correction is small, but is increasing with the volume of particles. The susceptibility of the foams without magnetic particles is negative and this can be interpreted as a diamagnetic behavior of PU matrix and air. The foam susceptibility χ increased at increasing filling factor ϕ_{Fe} as reported in Fig.5 for the relative magnetic permeability (μ_r =1+χ). Nonetheless the values are slightly different, and several parameters could explain this discrepancy. Relative permeabilities and susceptibilities were measured with two different techniques, on sample having same origin but with slightly different densities (Fig.3). Lastly, a difference in the clamping system of the samples may yield to the two results being somewhat different.

2.3.2 With compression. When the uniaxial compression is applied, the sample thickness is reduced from h_0 down to h. The measurements of the permeability of samples dependency on the deformation are plotted in the Fig.6a versus the relative change of thickness of the samples $|\varepsilon|=|(h-h_0)|/h_0$.

The permeabilities of samples without strain (ε=0) are the same as in Fig.5, in this case, permeability is a function of the filling factor ϕ_{Fe}. Unsurprisingly, the pure foam, which presented no magnetic behavior without strain $\mu_r(\varepsilon=0, \phi_{Fe}=0)=1$ in Fig.4-5, was not presenting any magnetic behavior under strain as well $\mu_r(\varepsilon>0, \phi_{Fe}=0)=1$ (Fig.6a). This curve can however provide an indication regarding the level of noise which remained within the Permeability Meter error range of ±0.001.

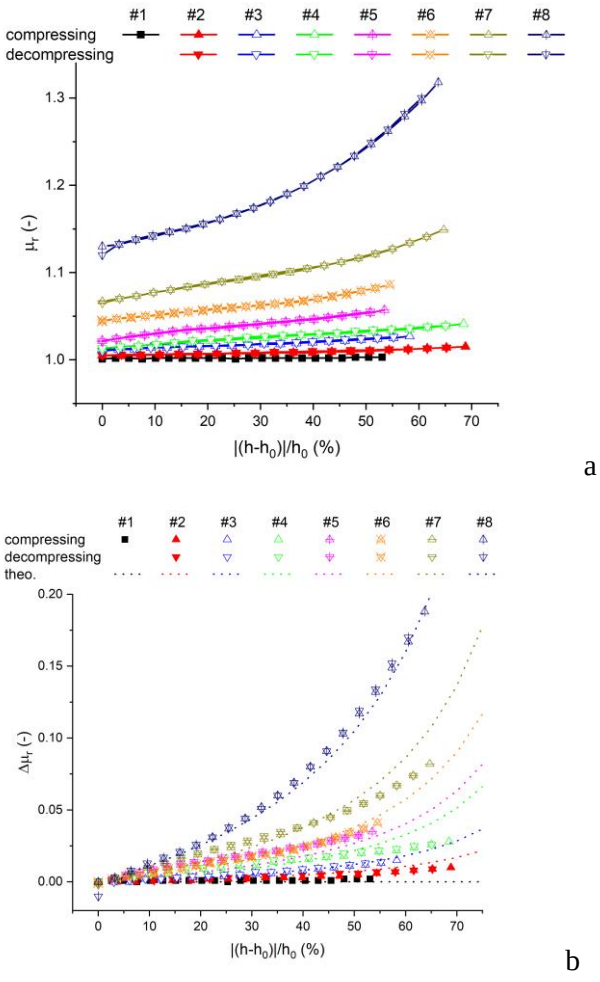

Fig.6. a) Permeabilities μ_r *of samples versus strain and b) relative change of permeabilities* $\Delta\mu_r$ *versus strain, dotted lines are theoretical curves obtained by using Eq.17.*

On the other hand, the Magneto-Rheological Foams filled by magnetic particles exhibit a clear dependency of the permeability with the deformation. This dependency increases with the Fe content. Moreover, for the samples with high content of Fe, #7 and #8, a non-linearity of permeability can be seen as $|\varepsilon|=|(h-h_0)|/h_0 > 50\%$. To explain this, the change of permeability $\Delta\mu_r$, defined as the difference between the deformed permeability $\mu_r(\varepsilon\neq0)$ and the non-deformed permeability $\mu_r(\varepsilon=0)$ of the Magneto-Rheological Foams, is isolated and may be expressed as:

$$\Delta\mu_r = \mu_r(\varepsilon \neq 0) - \mu_r(\varepsilon = 0) \qquad (10)$$

This term $\Delta\mu_r$ was calculated according to Eq.10 for all samples and are plotted in the Fig.6b.

As clearly seen in Fig.6b, all the Magneto-Rheological Foams samples have their permeabilities increased as they were compressed, $\Delta\mu_r(\varepsilon>0)>0$. Especially, sample #8 exhibited the largest relative change of $\Delta\mu_r\sim0.2$. In the case of anisotropic MRE experiencing shear strain applied perpendicularly to their anisotropic axis, the permeabilities were observed to decrease, i.e. $\Delta\mu_r(\gamma\neq0)<0$ [9-11, 16]. In this regards, a magnetic composite can be designed to achieve the desired change of permeability: a positive change by compression of MR Foams ($\Delta\mu_r(\varepsilon>0)>0$) or negative change by shear strain of anisotropic MREs ($\Delta\mu_r(\gamma\neq0)<0$).

From the Fig.6a and Fig.6b, the permeabilities of the Magneto-Rheological Foams are all observed to present no hysteresis. The MH loop presented in Fig.4 for each sample didn't show any magnetic hysteresis. Moreover, the deformation applied during these permeabilities measurements were done in a quasi-static way and small strain rate compression can explained the good mechanical properties of foams [27].

As previously stated for the magnetic saturation, the measured magnetization of composite is a quantity relating the direction of magnetic moments relatively to the applied magnetic field direction. The magnetization depends on the effective filling factor, but in a non-trivial compared to the saturation state. This is because the field produced by all the particles in the composite would also contribute into an effective magnetic field and particles orientation along the applied field is then more complicated. In general, the magnetic field generated by a single magnetized spherical particle is modelled, at the first order, as the dipolar field (~$1/r^3$) [12-13,16], so that the particle-particle interaction is highly nonlinear with their relative distance. This means that this particles field depends on the number of particles, thus the filling factor. By applying the compression, the resulting interaction should enhance the permeability as the inter-particle distance is reduced. However, the filling factor measured are quite small and the effective permeability could be well modelled by the MG law

which assumed no interaction between the particles. As the sample is being compressed, the sample volume is reduced this effect of reduction of volume to the magnetization has to be considered for understanding the measurements for these low filling factor samples. The more magnetic particles in the composite volume, the larger the magnetization is, as confirmed by Fig.5. This is also true for the permeability as seen in Fig.4. To extrapolate this, the composites being compressed, their volume are reduced, but the volume of the magnetic particles remained constant because they are nearly incompressible. Consequently, the magnetization increased. To model the compression effect on the composite magnetization, the effective filling factor is evaluated as function of the compression.

This effective compressed filling factor is firstly redefined as:

$$\begin{aligned}\phi_{Fe}(\varepsilon \neq 0) &= \frac{nV_p}{V_{tot}(\varepsilon \neq 0)} \\ &= \frac{nV_p}{V_{tot}(\varepsilon = 0) + \Delta V_{tot}(\varepsilon \neq 0)} \\ &= \phi_{Fe}(\varepsilon = 0)\frac{1}{1 + \frac{\Delta V_{tot}(\varepsilon \neq 0)}{V_{tot}(\varepsilon = 0)}}\end{aligned} \quad (11)$$

Where V_p is the volume of a particle, n is the total number of particle and V_{tot} is the volume of the sample. The change of the volume during the compression, $\Delta V(\varepsilon \neq 0)<0$, is then mechanically increasing the filling factor. To go further in the discussion, the volume change $\Delta V(\varepsilon \neq 0)$ can be expressed as function of the compression. The uniaxial compressive strain ε and the two lateral strains ε_t, assuming that they are the same, and the volume are related according to classic mechanical law as:

$$\begin{aligned}V_{tot}(\varepsilon \neq 0) &= V_{tot}(\varepsilon = 0) + \Delta V_{tot}(\varepsilon \neq 0) \\ &= V_{tot}(\varepsilon = 0)(1 + \varepsilon)(1 + \varepsilon_t)^2\end{aligned} \quad (12)$$

The corresponding strain ε and the lateral strains ε_t were experimentally extracted as described in [28] during the uniaxial compression of sample #6. Some pictures were taken at different compression levels and are presented in Fig.7a. From these two components, the relative change of volume $\Delta V(\varepsilon \neq 0)/V(\varepsilon=0)$ was calculated according to Eq.12 and the corresponding curve of is plotted in Fig.7b.

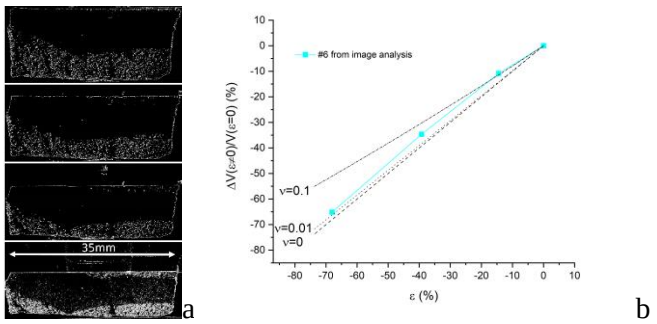

a b

Fig.7.a) Processed images of sample #6 under different stages of uniaxial compression and b) change of volume from processed images [28] of sample #6 as blue dots, relative change of volume added for comparison obtained as a function of the compression for all the magnetic foams where $\varepsilon_t = -\nu\varepsilon$ for different values of ν.

The Poisson's ratio ν is defined as the ratio of the longitudinal strain to the transverse strain: $\varepsilon_t = -\nu\varepsilon$. Injecting this relationship in Eq.12 could allow some simulated curves of $\Delta V(\varepsilon \neq 0)/V(\varepsilon=0)$ for different amplitude of ν. These curves, with selected low values of ν, were added in Fig.7b. This highlights the fact that the Poisson's ratio of foam is usually very small [28]. The foam relative change of volume is then approximated by a linear behavior with uniaxial compression ε; and by keeping the first order term of Eq. 12, the relative change of volume with the compression with the addition of the Poisson's ratio is finally approximated as:

$$\frac{\Delta V_{tot}(\varepsilon \neq 0)}{V_{tot}(\varepsilon = 0)} = (1 - 2\nu)\varepsilon \quad (13)$$

Fitting the curve from Fig.7b with Eq.13, the Poisson's ratio value is found to be $\nu \sim 0.03$. Such Poisson's ratio is quite typical for foams where hyperelastic modelling also confirmed the measurements of nonlinearity of ν with ε [28]: decreasing from ν=0.3 at ε =-5% down to ν=-0.02 at ε=-75%. This is however out of the scope of the present study and, in the following, the value of Poisson's ratio for a foam will be assumed to be ν=0 for simplicity of the model. Eq.13, with ν=0, is then providing a simple yet valid expression as $\Delta V(\varepsilon \neq 0)/V(\varepsilon=0)=\varepsilon$. This direct link between the relative change of volume and the compressive strain is then converted into an effective volume fraction of particles in the compressed samples by changing Eq.11 into:

$$\phi_{Fe}(\varepsilon \neq 0) = \phi_{Fe}(\varepsilon = 0)\frac{1}{1 + \varepsilon} \quad (14)$$

As previously stated, the filling factor of the composites are relatively small and the magnetic permeabilities are following the MG law (Eq.9) which is expressed with the effective filling factor (Eq.14) as:

$$\mu_r = 1 + \frac{3\phi_{Fe}(\varepsilon=0)\frac{1}{1+\varepsilon}}{1-\phi_{Fe}(\varepsilon=0)\frac{1}{1+\varepsilon}} = \frac{1+\varepsilon+2\phi_{Fe}(\varepsilon=0)}{1+\varepsilon-\phi_{Fe}(\varepsilon=0)} \quad (15)$$

The relative magnetic permeability change $\Delta\mu_r$ with ε is then expressed as:

$$\frac{\Delta\mu_r}{} = \frac{-3\varepsilon\phi_{Fe}(\varepsilon=0)}{\big(1-\phi_{Fe}(\varepsilon=0)\big)\big(1+\varepsilon-\phi_{Fe}(\varepsilon=0)\big)} \quad (16)$$

This equation is only a function of the non-deformed filling factor ϕ_{Fe} (ε=0) and the compression ε.

Finally, this expression can be rearranged by identifying in Eq.16 the non-deformed Maxwell-Garnett susceptibility χ (Eq.9) as:

$$\Delta\mu_r = \chi(\varepsilon=0)\frac{-\varepsilon}{(1-\phi_{Fe}(\varepsilon=0)+\varepsilon)} \quad (17)$$

Theoretical curves, using Eq.17 and the filling factor from Table 2, are plotted in Fig.6b together with the corresponding experimental data and a good agreement is found.

This model has only assumed a small filling factor which was confirmed by density and magnetic measurements; this small filling factor allows the use of the Maxwell Garnett for non-deformed samples. Uniaxial compression was observed to be highly compressive as the extraction of low Poisson's ratio confirmed (Fig.7b). These two approximations were then combined to obtain Eq.17 which fitted well the experimental data with few free parameters

2.4 Inductance variation with the compression

From Fig.7.b, it was observed a linear change of permeability for low applied compression range whereas for larger strain, the behavior was no longer linear. For sample #5, the linearity limit is up to nearly 40% for and up to 30% for sample #8. In this range of compression, the corresponding permeability curves are plotted in Fig.8.a and a linear fitting was performed on these two curves. The extracted linear coefficient are $d\mu_r/d\varepsilon$ = 5.8.10^{-2} for sample #5 and $d\mu_r/d\varepsilon$ = 15.4.10^{-2} for sample #8. As an approximate solution, this coeffient can be retrieved from the above model as variation of permeability (Eq.16) divided by the considered compression amplitude, yielding to:

$$\frac{\Delta\mu_r}{\varepsilon} = \frac{-3\phi_{Fe}(\varepsilon=0)}{\big(1-\phi_{Fe}(\varepsilon=0)\big)\big(1+\varepsilon-\phi_{Fe}(\varepsilon=0)\big)} \quad (18)$$

The corresponding linear coefficient values are 4.5.10^{-2} and 13.7.10^{-2} for samples #5 and #8 respectively in agreement with the experimental data.

For a solenoid, the value of the inductance L is proportional to the core material permeability μ_r as: $L=k\mu_r$, where k a constant taking into account the geometry and the number of turns. A small coil, with inductance L_0=26.47µH without sample, was placed on top of samples #5 and #8 for similar compression test. The same range of compression were used in the inductance measurements during compression test as for the permeability linear range. In Fig.8.b, these results are plotted as function of the compression. As the samples are deformed, the inductances are propotional to the strain. These data were fitted using a line and the extracted slopes were $dL/d\varepsilon$= 5.7.10^{-2} µH for sample #5 and $dL/d\varepsilon$ = 13.3.10^{-2} µH for sample #8. The relative permeabilities change with compression are in good agreement to the values found by inductance during compression. Hence, such results give good insight in terms of application example of the MR foam as strain sensor, featuring good sensitivity while being highly deformable.

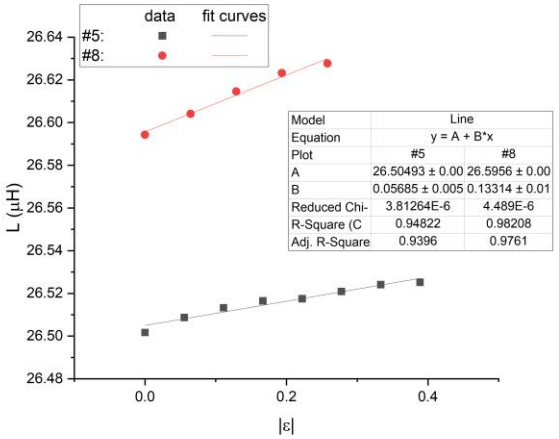

a

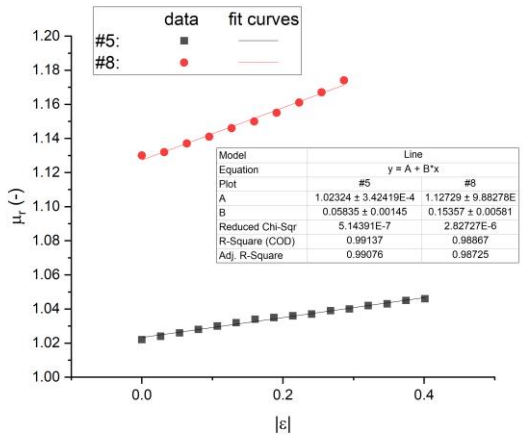

b

Fig.8. Example of permeability change induced by compression in two different samples a) and inductance change of a coil induced by compression for the same samples b).

3. Conclusion

In this article, the magnetic properties of a polyurethane foam filled by spherical Fe particles were measured as a function of a uniaxial compression. The volume fraction of particles in the composites were measured using two methods, density and magnetic saturation of the composite; the results show good agreements in the values. In this report, mainly small filling factor comsposite were achieved. The composite Poisson's ratio was measured using optical strain observation and the resulting value was found to be small enough to approximate the composite as a compressible medium.

The magnetic relative permeability characterization, with direct permeability meter under this uniaxial compression is provided for different filling factor values. These permeabilities were found to be increasing with the compression amplitude. The low filling factor and the low Poisson's ratio allowed to model these permeabilities by a simple model based on the Maxwell Garnett mixing rule. This model, with the filling factor as only parameter was providing significantly good prediction compared to the experimental ones. These permeability change with the compression was confirmed by inductance measurements of a coil placed above the sample under compression.

These results show the interest of considering elastomeric foams rather than elastomeric massive materials, as (i) there are easily and highly deformable, (ii) their apparent Poisson's ratio is close to 0 (contrary to massive elastomers which are almost non compressible: ν~0.5). Such study provided magnetic behavior of a material nearly fully compressible. Elastomeric foams are then good candidates to be used in applications like actuators, energy harvesting and so on as their properties are varying significantly, while featuring low cost and easy processability. To this end, a simple yet sensitive strain sensor through inductance variation has been demonstrated.

In future work, the larger filling factor will be discussed as the interaction was not considered in the Maxwell-Garnett mixing rule. Similarly, the compressibility effect, for sample with Poisson'ratio $0< \nu <0.5$ can also be considered in future work.

Acknowledgements

The authors greatly acknowledge the support of this work by the Tohoku University Research Program "Frontier Research in Duo" (FRiD).

The author is grateful to Pr. Fumio Narita, for the possibility of using the VSM equipment and to Pr. Fumio Narita and Mr. Kenichi Katabira for their assistance.

The author is grateful to Chrystelle Bernard for fruitful discussion.

M Lallart gratefully acknowledges the support of JSPS through invitational fellowship grant number L19530, as well as the support of INSA-Lyon through the CRCT program.

References

[1] Li Y., Li J, Li W. and Du H. 2014 *Smart Mater. Struct.* **23** 123001

[2] Samal S., Škodová M., Abate L. and Blanco I. 2020 *Appl. Sci.* **10** 4899

[3] Kumar J., Paul P.S., Raghunathan G. and Alex D.G. 2019 *International Journal of Mechanical and Materials Engineering* **14:13** 1-18

[4] Popplewell J. and Rosensweig R.E. 1996 *J. Phys. D: Appl. Phys* **29** 2297

[5] Diguet G., Beaugnon E. and Cavaillé J.Y. 2010 *Journal of Magnetism and Magnetic Materials* **322** 3337–3341

[6] Diguet G., Beaugnon E. and Cavaillé J.Y 2009 *Journal of Magnetism and Magnetic Materials* 321 396-401

[7] Martin J.E., Anderson R.A., Read D. and Gulley G. 2006 *Phys. Rev. E* **74** 051507.

[8] Rosensweig R.E, Ferrohydrodynamics. Dover Publications inc., ISBN 9780486678344

[9] Sebald G., Nakano M., Lallart M., Tian T., Diguet G. and Cavaille J.Y. 2017 *Science and Technology of Advanced Materials* **18** 766-778

[10] Lallart M., Sebald G., Diguet G., Cavaille J.Y. and Nakano M. 2017 *J. Appl. Phys.* **122** 103902

[11] Diguet G., Sebald G., Nakano M., Lallart M. and Cavaille J.Y. 2020 *Smart Mater. Struct.* **29** 075017

[12] Martin J.E., Venturini E., Odinek J. and Anderson R.A., 2000 *Phys. Rev. E* **61** 2818

[13] Yin H.M. and Sun L.Z. 2006 *Acta Materialia* **54** 2317–2323

[14] Varga Z., Filipcsei G. and Zrínyi M. 2006 *Polymer* **47** 227–233

[15] Boczkowska A., Awietjan S.F. and Wroblewski R. 2007 *Smart Mater. Struct.* **16** 1924–1930

[16] Diguet G., Sebald G., Nakano M., Lallart M. and Cavaille J.Y. 2019 *Journal of Magnetism and Magnetic Materials* **481** 39–49
[17] Sorrentino L., Aurilia M., Forte G. and Iannace S. 2008 *Advances in Science and Technology* **54** 123-126
[18] Sorrentino L., Aurilia M., Forte G. and Iannace S. 2011 *Journal of Applied Polymer Science* **119** 1239–1247
[19] Ju B.X., Yu M., Fu J., Yang Q., Liu X.Q. and Zheng X. 2012 *Smart Mater. Struct*. **21** 035001
[20] Gong Q., Wu J., Gong X., Fan Y. and Xia H. 2013 *Royal Society of Chemistry Adv.* **3** 3241-3248
[21] Plachy T., Kratina O., Sedlick. M, 2018 *Composite Structures* **192** 126-130.
[22] Cvek M., Kuktalkova E., Mouchka R., Urbanek P., Sedlick M., 2020 *International Journal of Mechanical Sciences* **183** 105816
[23] Irwin T.D., Li W., Diaz A. 2020 *International Conference on Environmental Systems* 128
[24] Sedlacik M., Pavlinek V., Vyroubal R., Filip P. 2013 *Smart Mater. Struct*. **22** 035011.
[25] Garnett J.C.M. 1904 *Phil. Trans. Roy. Soc. A* 385-420
[26] P. Prozorov and Kogan V.G. 2018 *Physical review applied* **10** 014030
[27] Saha M.C., Mahfuz H., Chakravarty U.K., Uddin M., Kabir Md. E., Jeelani S. 2005 *Materials Science and Engineering A* **406** 328-336.
[28] Widdle Jr. R.D., Bajaj A.K. and Davies P. 2008 *International Journal of Engineering Science* **46** 31-49